



ELSEVIER

Contents lists available at ScienceDirect

Physica B

journal homepage: www.elsevier.com/locate/physb

Formation of MgZnO alloy under thermodynamic conditions



I.V. Markevich, T.R. Stara*, A.V. Kuchuk, Yu.O. Polishchuk, V.P. Kladko

V. Lashkaryov Institute of Semiconductors Physics, National Academy of Sciences of Ukraine, Pr. Nauky, 41, 03028 Kyiv, Ukraine

ARTICLE INFO

Available online 16 May 2014

Keywords:

MgZnO ceramics
Photoluminescence
X-ray diffraction

ABSTRACT

Mg_xZn_{1-x}O ceramics with $x=0.10, 0.15, 0.20, 0.25$ and 0.30 were sintered at $T_s=700\text{--}1250$ °C. Photoluminescence (PL) and PL excitation (PLE) spectra as well as X-ray diffraction patterns were measured at 293 K. Bandgap width was evaluated from the position of PLE peak. Non-monotonous dependence of PLE peak position on T_s was observed for all used x . This effect was concluded to be caused by the formation of cubic phase side by side with hexagonal one and the enhancement of this process with increasing T_s , which resulted in the decrease of Mg content in the hexagonal phase at $T_s > 1000$ °C. Temperature range of 1000–1050 °C was found to be the optimum one for the formation of hexagonal MgZnO alloy at used x . It was shown that $x=0.20$ was the solubility limit of MgO in hexagonal Mg_xZn_{1-x}O ceramics.

© 2014 Elsevier B.V. All rights reserved.

1. Introduction

ZnO-based materials are promising candidates for optical device applications. In recent years, much attention is attracted to the preparation and investigation of MgZnO ternary systems. By alloying with MgO, bandgap of ZnO can be extended to about 7.0 eV, which gives the possibility to shift active spectral range of lasers, light emitting diodes and photo-detectors into deep ultraviolet [1]. Besides, adding MgO to ZnO was found to result in the enhancement of band-edge emission [2].

Because of crystal structure dissimilarity between hexagonal wurtzite ZnO and cubic rock-salt MgO, these two oxides do not show a complete solubility over the entire composition range. It is usually assumed that, with increasing Mg content, at first only alloys with wurtzite structure appear, then separation of wurtzite and rock-salt phases takes place, and at last rock-salt structure alloys are formed [4–6]. However, the upper limit of Mg content in Mg_xZn_{1-x}O alloy that still keep wurtzite structure has not been established reliably. Quite different values of this limit, such as $x=0.1$ [6], $x=0.15$ [7], $x=0.18$ [8], $x=0.20$ [9], $x=0.33$ [3,11], $x=0.46$ [12] and $x=0.49$ [13] were reported. In addition, bandgap width reported in different works for the same x values varies noticeably. Therefore, further study of MgO and ZnO alloying process is required.

It should be noted that the majority of investigators have dealt with thin films [1–7,9–22] and only a few works have been performed on ceramics [8,24–26]. At the same time, the latter is

a very suitable material for research in MgZnO alloy formation due to simplicity of its preparation, facility of modification of preparation conditions in a wide range and the ability to study alloying process under thermodynamic conditions. In the present paper, the influence of Mg content and sintering temperature T_s on crystal structure and luminescence of MgZnO ceramics was investigated.

2. Experimental procedure

The samples were formed of the mixture of ZnO (99.99% purity) and MgO (99.98% purity) powders with distillate water, Mg content being 10; 15; 20; 25 and 30 at%. After drying at room temperature, the samples were sintered at $T_s=700\text{--}1250$ °C in air for 3 hours and cooled with the furnace. The average sizes of sintered ceramics were $10 \times 3 \times 2$ mm³. After cooling, the samples were cut transversally and defect-related photoluminescence (PL) spectra in 400–800 nm range and PL excitation (PLE) spectra in 250–400 nm range were measured from cleft surface at 293 K using Xe-lamp light passing through grating monochromator as exciting source.

The structural properties of MgZnO samples were studied using X'Pert Pro MPD X-ray diffractometer with CuK α wavelength ($\lambda=0.15418$ nm).

3. Results and discussion

In all prepared samples, broad PL band in green–orange spectral region centered at around 530–570 nm was observed under

* Corresponding author. Tel.: +38 44 5256340; fax: +38 44 5258342.
E-mail address: stara_t@ukr.net (T.R. Stara).

excitation by 250–300 nm light that produced band-to-band transitions. PLE spectra measured at a fixed wavelength corresponding to PL band maximum are shown in Fig. 1. It is known that, in ZnO and hexagonal MgZnO alloys, excitons contribute essentially to the fundamental band-gap transitions at room temperature and PLE spectra of defect-related PL exhibit sharp peaks whose positions coincide with that of absorption and emission bands related to free excitons [27,28]. Thus, band-gap width of prepared ceramics $E_g = hv_m + E_{ex}$, where hv_m is energetic position of PLE peak and E_{ex} is exciton binding energy. The later is about 60 meV in ZnO and has been found to remain, in fact, unchanged under alloying ZnO with MgO up to $x=0.37$ [15].

In PLE spectra of all MgZnO samples sintered at $T_s=700^\circ\text{C}$, the only peak was observed at $\lambda_m=374\text{ nm}$, which is about the position of PLE peak in ZnO. So, one can suggest that alloying process did not occur in fact at this temperature. At $T_s=800^\circ\text{C}$ the other PLE peak at shorter wavelengths appeared side by side with that at $\lambda_m=374\text{ nm}$, i.e. the formation of MgZnO alloy began already. With further increasing T_s , the longer wavelength peak decreased gradually and disappeared, whereas PLE peak related to MgZnO alloy shifted at first to shorter wavelength and then moved in opposite direction. This behavior of PLE spectra for the samples with $x=0.20$ is shown in Fig. 1(a and b).

The dependences of PLE peak position on T_s for samples with different x are plotted in Fig. 2. One can see that PLE peak position shifts to shorter wavelength with increasing Mg content up to $x=0.20$ and then maintains unchanged, which indicates that further Mg incorporation in ZnO lattice does not occur. Obviously, it can be concluded that $x=0.20$ is solubility limit of MgO in ZnO lattice under thermodynamic conditions and, at this Mg content, $E_g=3.64+0.06=3.7\text{ eV}$. It should be thought, therefore,

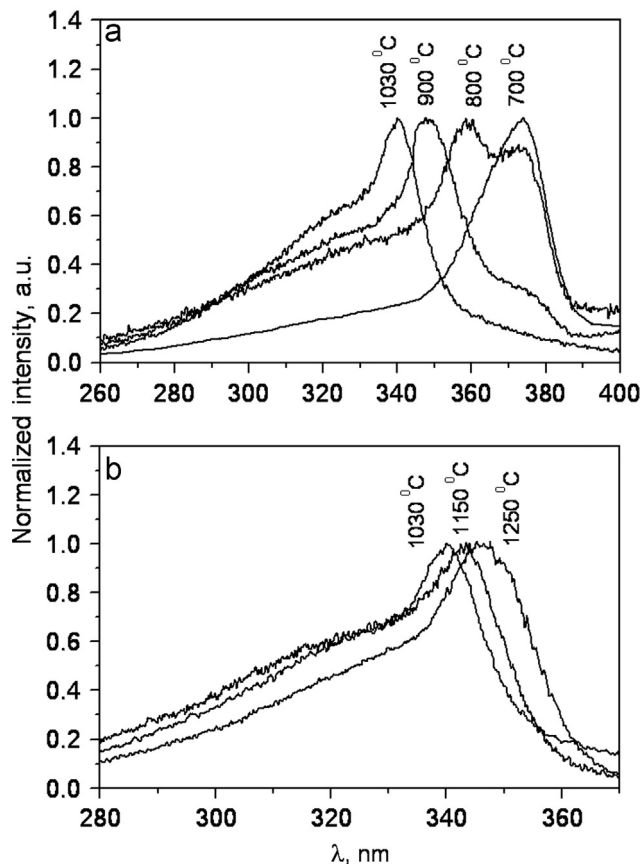


Fig. 1. PLE spectra of $\text{Mg}_{0.20}\text{Zn}_{0.80}\text{O}$ samples sintered at (a) 700–1030 and (b) 1030–1250 $^\circ\text{C}$.

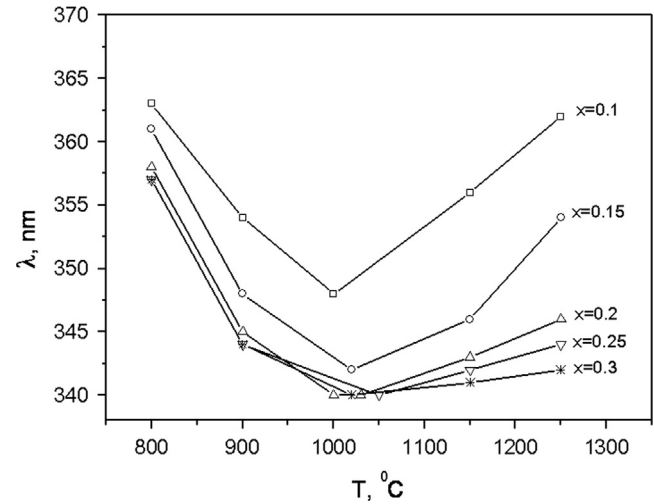


Fig. 2. Dependences of PLE peak positions λ_m on sintering temperature T_s for ceramics with different x .

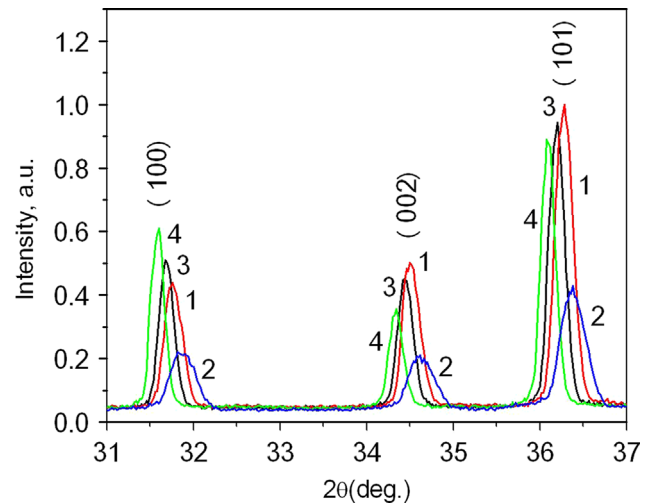


Fig. 3. XRD patterns of $\text{Mg}_{0.10}\text{Zn}_{0.90}\text{O}$ ceramics sintered at 920 (1), 1000 (2), 1150 (3) and 1250 $^\circ\text{C}$.

that wurtzite structure MgZnO films with $x > 0.20$ should be in metastable state. In fact, in these films prepared at relatively low temperatures (200–700 $^\circ\text{C}$), separation of ZnO-based and MgO-based phases was often observed after heating to 800–1000 $^\circ\text{C}$ [7,15,16]. Such metastability can explain, in particular, the variety of E_g values reported for $\text{Mg}_x\text{Zn}_{1-x}\text{O}$ alloys with the same x .

As it follows from Figs. 1 and 2, non-monotonous dependence of PLE peak position on T_s is observed, namely, λ_m blueshift up to $T_s=1000\text{--}1050^\circ\text{C}$ and its following redshift at higher temperatures occur. Therefore, at $T_s > 1050^\circ\text{C}$, bandgap shrinkage takes place, which implies the decrease of Mg content in MgZnO hexagonal phase responsible for measured PL. It is seen from Fig. 2 that the strongest bandgap shrinkage is observed for the samples with $x=0.10$ and this effect weakens gradually with increasing x . The change of hexagonal phase composition depending on T_s is confirmed by XRD measurements. Shown in Fig. 3 XRD spectra for samples with $x=0.10$ sintered at different T_s exhibit the shift of (1 0 0), (0 0 2) and (1 0 1) hexagonal phase peaks at first to higher and then to lower angles, which reveals the initial rise and following reduction of Mg content in the hexagonal phase.

It should be noted that non-monotonous dependence of bandgap width on annealing temperature in hexagonal phase

MgZnO alloys was earlier observed for thin films [6,7,16,17,22] and was accounted for by the effect of MgO segregation, in particular, because of Mg departure due to the replacement of Mg atoms from sites to interstitials and their following gathering on grain boundaries [7,16,24]. To elucidate the origin of the process responsible for the decrease of Mg content in the hexagonal phase ceramics at $T_s > 1050$ °C, XRD patterns for $Mg_xZn_{1-x}O$ samples with different x as well as for the initial ZnO and MgO powders were measured (Fig. 4). It is seen that in all sintered samples both ZnO-based hexagonal phase $\{(1\ 0\ 0), (0\ 0\ 2), (1\ 0\ 1), (1\ 0\ 2) \text{ and } (1\ 1\ 0)\}$ peaks and MgO-based cubic one $\{(2\ 0\ 0) \text{ and } (2\ 2\ 0)\}$ peaks are present. The intensities of cubic-phase peaks are very low at $x=0.10$ and enhance gradually with increasing x . This enhancement becomes more essential for $x > 0.20$ when, in accordance with PLE measurements, MgO content in the initial mixture exceeds its solubility limit in the hexagonal phase.

Displayed in Fig. 4 XRD spectra show, that $(2\ 0\ 0)$ and $(2\ 2\ 0)$ cubic phase peaks in prepared ceramics are shifted toward shorter angles with respect to their location in MgO. This fact indicates that the incorporation of Zn in MgO lattice and the formation of cubic phase MgZnO alloy occur, whereas segregation of MgO does not take place. The latter, however, can be observed at higher T_s : the departure of Mg from the bulk of the sample and its accumulation on the surface was found to be initiated in $Mg_{0.1}Zn_{0.9}O$ ceramics at $T_s > 1300$ °C [24].

Since the cubic phase appears when MgO content in the initial mixture ($x=0.1$) is essentially lower than its solubility limit in the hexagonal phase ($x=0.2$), one can conclude that not phase separation but simultaneous formation of hexagonal and cubic phases occur under sintering. Obviously, it is the formation of cubic phase that results in non-monotonous dependence of E_g on T_s . In fact, the emergence of cubic MgZnO alloy side by side with hexagonal one signifies that some parts of MgO and ZnO are removed from the initial mixture and, so, their contents in the

hexagonal phase must change. Cubic phase $Mg_xZn_{1-x}O$ alloy has been shown to form at $x > 0.50$ [4,16], which means that removed quantity of MgO must exceed that of ZnO. Taking in account this correlation as well as essentially lower content of MgO in the hexagonal phase with respect to that of ZnO, one should conclude that the formation of cubic phase will cause the decrease of MgO relative share in the hexagonal phase. The formation of cubic MgZnO alloy was found to intensify sharply with increasing temperature [10,11,23]. In $Mg_xZn_{1-x}O$ ceramics, cubic phase was reported to be detected only at $T_s > 900$ °C even for the samples with $x=0.60$ and the contribution of this phase enhanced drastically with increasing temperature at $T_s > 1000$ °C [23]. Swift enhancement of cubic phase contribution with the rise of substrate temperature was also observed in MgZnO films [10,11]. Since at $T_s > 1000$ °C the formation of cubic phase intensifies, the quantities of ZnO and MgO taking part in this process will rise with increasing T_s . In the samples with low x , however, the removal of ZnO will still remain insignificant and will slightly influence ZnO content in the hexagonal phase. At the same time, the relative decrease of MgO content in this phase will be considerably higher and will noticeably enhance with increasing T_s . The higher x the lower the relative decrease of MgO content and the higher that of ZnO one in the hexagonal phase, which should result in the weakening of non-monotony in E_g dependence on T_s . At $x > 0.20$, the “redundant” MgO that takes no part in the formation of the hexagonal phase can contribute to the cubic one and further weakening of this non-monotony can be expected. It is the effect that was observed (Fig. 2).

It should be noted that the emergence of detectable cubic phase peaks in XRD patterns is often considered as the evidence of exceeding MgO content in the initial composition over its solubility limit in ZnO [3,6,9,25,26]. Our investigations show, however, that, although cubic phase peaks are present in XRD spectra at $x=0.1$, further solution of MgO in ZnO and the broadening of E_g occur at $x=0.15$ and $x=0.20$. Correct evaluation of MgO solubility limit in ZnO can, obviously, be made from the shift of hexagonal phase XRD peaks toward higher angles with respect to ZnO ones. At the same time, reverse shift of these peaks due to the decrease of Mg content in hexagonal phase with increasing T_s should be also taken into account. So, more precise data can be obtained at higher x when this effect is enough weak. The shift of cubic phase XRD peaks toward lower angles with respect to MgO ones for all used x means that intrusion of both Mg into ZnO lattice and Zn in MgO one begin from the outset of alloying process. Thus, the change of hexagonal phase composition with increasing T_s is not caused by the departure of Mg from earlier formed hexagonal MgZnO alloy but is due to the “competition” of hexagonal and cubic phase formation processes. At comparatively low temperatures, the formation of hexagonal phase is predominant process even when x exceeds the value of MgO solubility limit in ZnO [10,23]. On the other hand, as our investigations show, the formation of cubic phase takes place at higher temperatures even when x is essentially lower of this value. It was recently found that native defects [20,21] and some impurities [11] can also influence the formation of MgZnO alloy.

To find the optimal conditions for both hexagonal and cubic phase formation in MgZnO ceramics, further investigations of the influence of sintering duration, heating and cooling velocities as well as different impurities on this process are planned.

4. Conclusion

$Mg_xZn_{1-x}O$ ceramics with $x=0, 0.10, 0.15, 0.20, 0.25$ and 0.30 were sintered at 700–1250 °C. Bandgap width E_g in obtained samples was evaluated from the energetic position of photoluminescence

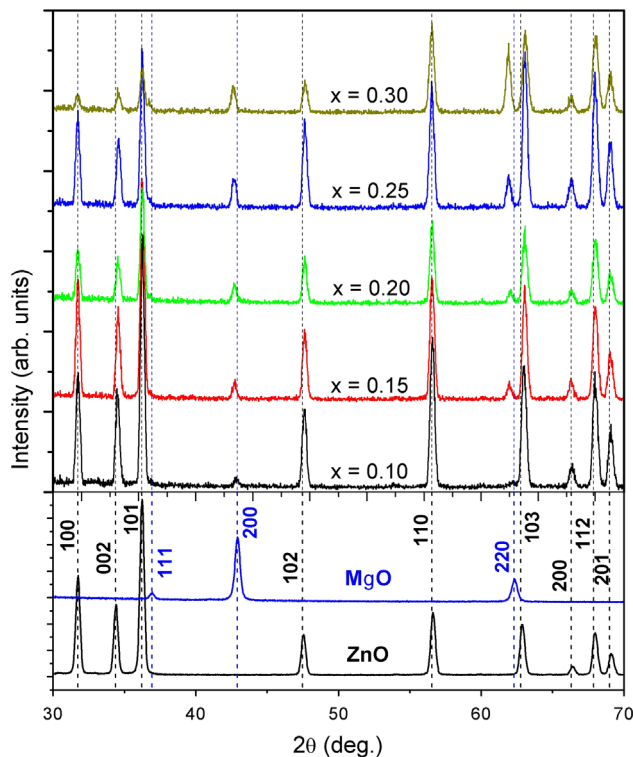


Fig. 4. XRD patterns for the initial ZnO and MgO powders (lower curves) and $Mg_xZn_{1-x}O$ ceramics with $x=0.10, 0.15, 0.20, 0.25$ and 0.30 sintered at 1000–1030 °C (upper curves).

excitation peak. Formation of hexagonal structure MgZnO alloy was found to begin at 800 °C. XRD patterns showed that, side by side with hexagonal phase, some share of cubic one was present in the samples with $x \geq 0.10$. Non-monotonous dependence of E_g on sintering temperature, namely, its initial broadening up to $T_s = 1000\text{--}1050$ °C and following shrinkage at $T_s > 1050$ °C, was observed for all used x , the non-monotony being the strongest for $x = 0.1$ and weakening with increasing x . This effect was shown to result from the decrease of MgO content in the hexagonal phase MgZnO alloy due to the formation of cubic phase simultaneously with hexagonal one. It was concluded that the formation of cubic phase began from the outset of the alloying process, the relative contribution of cubic phase increasing with the rise of T_s and MgO content in the initial mixture. It was stated that the appearance of cubic phase peaks in MgZnO alloy XRD patterns can not be considered as the evidence that MgO content in the initial composition exceeds its solubility limit in ZnO. Correct evaluation of this value can, obviously, be made from the shift of hexagonal phase XRD peaks with respect to ZnO ones, and the decrease of MgO content in the hexagonal phase with increasing T_s should be also taken into account. Obtained results show that $x = 0.20$ is solubility limit of MgO in hexagonal structure MgZnO alloy under thermodynamic conditions.

Acknowledgment

This research has been financially supported by National Academy of Sciences of Ukraine (projects III-4-11 and III-10-12).

References

- [1] Y. Kozuka, A. Tsukazaki, M. Kawasaki, *Appl. Phys. Rev.* 1 (2014) 011303.
- [2] H. Shibata, H. Tampo, K. Matsubara, A. Yamada, K. Sakurai, S. Ishizuka, S. Niki, *Appl. Phys. Lett.* 90 (2007) 124104.
- [3] A. Ohtomo, M. Kawasaki, T. Koida, K. Masubuchi, H. Koinuma, *Appl. Phys. Lett.* 72 (1998) 2466.
- [4] Z. Vashaei, T. Minegishi, H. Suzuki, T. Hanada, M.W. Cho, T. Yao, *J. Appl. Phys.* 98 (2005) 054911.
- [5] R. Schmidt-Grund, A. Carstens, B. Rheinlander, D. Spemann, H. Hochmut, G. Zimmermann, M. Lorenz, M. Grundmann, C.M. Herzinger, M. Schubert, *J. Appl. Phys.* 99 (2006) 123701.
- [6] Q. Shi, J. Zhang, D. Zhang, Ch. Wang, B. Yang, B. Zhang, W. Wang, *Mater. Sci. Eng., B* 177 (2012) 689.
- [7] A. Ohtomo, R. Shiroki, I. Ohkubo, H. Koinuma, M. Kawasaki, *Appl. Phys. Lett.* 75 (1999) 4088.
- [8] C. Bergstein, NNIN R.E.U. Research Accomplishments (2008) 150.
- [9] A. Singh, A. Vij, D. Kumar, P.K. Khanna, M. Kumar, S. Gautam, K.H. Chae, *Semicond. Sci. Technol.* 28 (2013) 025004.
- [10] P. Bhattacharya, R.R. Das, R.S. Katiuar, *Appl. Phys. Lett.* 83 (2003) 2010.
- [11] L. Su, Yu Zhu, Q. Zhang, M. Chen, Xu Ji, T. Wu, X. Gui, B. Pan, R. Xiang, Z. Tang, *J. Phys. D: Appl. Phys.* 46 (2013) 245103.
- [12] J.S. Liu, C.X. Shan, S.P. Wang, B.H. Li, Z.Z. Zhang, D.Z. Shen, *J. Cryst. Growth* 347 (2012).
- [13] W.I. Park, G.-Ch Yi, H.M. Jang, *Appl. Phys. Lett.* 79 (2001) 2022.
- [14] C.W. Teng, J.F. Muth, U. Ozgur, M.J. Ber gmann, H.O. Everitt, A.K. Sharma, C. Jin, J. Narayan, *Appl. Phys. Lett.* 76 (2000) 979.
- [15] S. Chooapun, R.D. Vispute, W. Yang, R.P. Sharma, T. Venkatesan, H. Shen, *Appl. Phys. Lett.* 80 (2002) 1529.
- [16] M. Wang, E.J. Kim, S. Kim, J.S. Chung, I.-K. Yoo, E.W. Shin, S.H. Hahn, Ch Park, *Thin Solid Films* 516 (2008) 1124.
- [17] D.Y. Jiang, D.Z. Shen, K.W. Liu, C.X. Shan, Y.M. Zhao, T. Yang, B. Yao, Y.M. Lu, J.Y. Zhang, *Semicond. Sci. Technol.* 23 (2008) 035002.
- [18] W. Wei, C. Jin, R.J. Narayan, *J. Electron. Mater.* 38 (2009) 613.
- [19] K. Tang, L.J. Wang, J. Huang, R. Hu, J.J. Zhang, W.M. Shi, Y.B. Xia, *Physics Procedia* 32 (2012) 245.
- [20] A. Agrawal, T.A. Dar, D.M. Phase, P. Sen, *J. Cryst. Growth* 384 (2013) 9.
- [21] S. Han, Y.K. Shao, Y.M. Lu, P.J. Cao, F. Jia, Y.X. Zeng, W.J. Liu, D.L. Zhu, X.C. Ma, *J. Alloys Compd.* 559 (2013) 209.
- [22] D.P. Xiong, X.G. Tang, W.R. Zhao, Q.X. Liu, Y.H. Wang, S.L. Zhou, *Vacuum* 89 (2013) 254.
- [23] J.L. Morrison, J. Huso, D. Thapa, M. Huso, M.G. Norton, L. Bergman, *J. Mater. Sci.: Mater. Electron.* 23 (2012) 437.
- [24] J. Zhung, Z.h. Zhang, T. Wang, *Chem. Mater.* 16 (2004) 768.
- [25] P. Kumar, J.P. Singh, Y. Kumar, A. Gaur, H.K. Malic, K. Asokan, *Curr. Appl. Phys.* 12 (2012) 1166.
- [26] Z.J. Othman, A. Matoussi, F. Fabbri, F. Rossi, G. Salviati, *Appl. Phys. A* (2014) 10.1007/s00339-014-8279-5.
- [27] J.H. Kang, Y.R. Park, K.J. Kim, *Solid State Commun.* 115 (2000) 127.
- [28] I.V. Markevich, V.I. Kushnirenko, L.V. Borkovska, B.M. Bulakh, *Phys. Status Solidi C* 7 (2010) 1605.